The Astrophysical Journal, 755:14 (12pp), 2012 August 10 doi:10.1088/0004-637X/755/1/14


# A TALE OF DWARFS AND GIANTS: USING A $z = 1.62$ CLUSTER TO UNDERSTAND HOW THE RED SEQUENCE GREW OVER THE LAST 9.5 BILLION YEARS*

Gregory H. Rudnick[1], Kim-Vy Tran[2], Casey Papovich[2], Ivelina Momcheva[3,5], and Christopher Willmer[4]
[1] Department of Physics and Astronomy, The University of Kansas, Malott room 1082, 1251 Wescoe Hall Drive, Lawrence, KS 66045, USA; grudnick@ku.edu
[2] Department of Physics and Astronomy, George P. and Cynthia Woods Mitchell Institute for Fundamental Physics and Astronomy, Texas A&M University, College Station, TX 77843-4242, USA
[3] Observatories, Carnegie Institution of Washington, 813 Santa Barbara Street, Pasadena, CA 91101, USA
[4] Steward Observatory, University of Arizona, 933 N. Cherry Avenue, Tucson, AZ 85721, USA
*Received 2011 December 12; accepted 2012 March 19; published 2012 July 20*

## ABSTRACT

We study the red sequence in a cluster of galaxies at $z = 1.62$ and follow its evolution over the intervening 9.5 Gyr to the present day. Using deep $YJK_s$ imaging with the HAWK-I instrument on the Very Large Telescope, we identify a tight red sequence and construct its rest-frame $i$-band luminosity function (LF). There is a marked deficit of faint red galaxies in the cluster that causes a turnover in the LF. We compare the red-sequence LF to that for clusters at $z < 0.8$, correcting the luminosities for passive evolution. The shape of the cluster red-sequence LF does not evolve between $z = 1.62$ and $z = 0.6$ but at $z < 0.6$ the faint population builds up significantly. Meanwhile, between $z = 1.62$ and 0.6 the inferred total light on the red sequence grows by a factor of $\sim$2 and the bright end of the LF becomes more populated. We construct a simple model for red-sequence evolution that grows the red sequence in total luminosity and matches the constant LF shape at $z > 0.6$. In this model the cluster accretes blue galaxies from the field whose star formation is quenched and who are subsequently allowed to merge. We find that three to four mergers among cluster galaxies during the 4 Gyr between $z = 1.62$ and $z = 0.6$ match the observed LF evolution between the two redshifts. The inferred merger rate is consistent with other studies of this cluster. Our result supports the picture that galaxy merging during the major growth phase of massive clusters is an important process in shaping the red-sequence population at all luminosities.

*Key words:* galaxies: clusters: general – galaxies: evolution – galaxies: formation – galaxies: high-redshift – galaxies: stellar content

## 1. INTRODUCTION

Understanding the formation of passive galaxies is an enduring problem in astronomy. These galaxies have very low star formation rates (SFRs), little or no cold gas, and dominate the population of massive galaxies in the local universe (e.g., Kauffmann et al. 2003). Their colors are uniformly red and they lie in a distinct region of color–magnitude (or color–mass) space called the red sequence. Studies of local passive galaxies indicate that their stellar populations are very old (e.g., Bower et al. 1992, 1998), with the most massive passive galaxies having the oldest mean stellar ages (e.g., Thomas et al. 2005; Gallazzi et al. 2006; Thomas et al. 2010, but see Trager et al. 2008). A problem with these studies is that it is not immediately apparent how to disentangle the ages of the stars from the time at which they assembled into present-day galaxies. In dramatic examples of the pitfalls that are present, Lauer (1988) and Rines et al. (2007) find observational evidence for past and ongoing mergers of old stellar systems in brightest cluster galaxies (BCGs). This behavior is echoed in the semianalytic model of De Lucia & Blaizot (2007) who show that BCGs have old stellar ages but relatively recent epochs where the mass was physically assembled. More recently, however, observations have shown that the observed stellar mass in BCGs has remained constant since $z \sim 1$ (Whiley et al. 2008; Collins et al. 2009; Stott et al. 2010, 2011), in contrast to the model predictions and the implications from the merger remnants seen in low-redshift BCGs. This highlights the difficulties inherent in interpreting the evolution of massive galaxies strictly using studies of the local universe.

Direct lookback studies of passive galaxies shed some light on their origin and evolution. For example, van der Wel et al. (2005) use fundamental plane observations of field galaxies to determine that low-mass red galaxies at $z < 1$ have younger mean stellar ages than their more massive counterparts, similar to what is seen from the local studies referred to above. In addition, a population of passive galaxies is seen as far back as $z \sim 2$ (Labbé et al. 2005; Daddi et al. 2005a; Cassata et al. 2008; Kriek et al. 2008; Brammer et al. 2009), indicating that at least some passive galaxies already were in place by that time, only 3.3 Gyr after the big bang. Despite their early presence on the stage, however, the number densities of passive galaxies evolved dramatically at $z < 2$ (Labbé et al. 2005; Kriek et al. 2008) with a factor of $\sim$2 in growth of number and mass densities at $z < 1$ (Bell et al. 2004; Brown et al. 2007; Faber et al. 2007; Taylor et al. 2009; Brammer et al. 2011). It is debated as to whether this growth was dependent on galaxy mass. While some works have shown that the rate of growth in the red galaxy population at $z < 1$ is slower in more massive galaxies (Cimatti et al. 2006; Brown et al. 2007; Faber et al. 2007), Brammer et al. (2011) do not find a strong mass dependence in number evolution of galaxies selected to have low SFRs. Nonetheless, Brammer et al. (2011) and Bundy et al. (2006) still find evidence for some mass–dependent evolution, as there is a stellar mass at which the passive and star-forming populations have equal density and this limit evolves to lower mass with the passing of cosmic time.

The most favored explanation for this growth in the total number of red-sequence galaxies is via the transformation of

* Based on observations obtained at the European Southern Observatory using the ESO Very Large Telescope on Cerro Paranal through ESO program 386.A-0514(A).
[5] Currently at Department of Astronomy, 260 Whitney Avenue, Yale University, New Haven, CT 06511, USA.

star-forming galaxies to passive ones, following a quenching episode (Blanton 2006; Bundy et al. 2006; Faber et al. 2007; Brammer et al. 2011). In general, this conclusion is consistent with the observed growth in number density on the red sequence and the constant number density of blue star-forming galaxies. Unfortunately, however, the quenching mechanism has not been conclusively identified and there are not enough bright blue galaxies at $z < 1.5$ to account for the observed evolution in the massive red-sequence population, if these blue galaxies were simply to fade onto the red sequence (e.g., Bell et al. 2004). One scenario to explain the growth of massive red galaxies without massive star-forming progenitors is to grow them via the mergers of low-mass galaxies. These mergers have to be dissipationless (or "dry") in order to preserve the red colors, isophote shapes, and low SFRs of the massive galaxies (e.g., Bell et al. 2004; Faber et al. 2007). Such a dry merging scenario has the added effect that it can grow the sizes of passive galaxies, which may explain the large evolution in sizes implied by some direct lookback studies (Daddi et al. 2005b; McIntosh et al. 2005; Trujillo et al. 2006; van Dokkum et al. 2008; van der Wel et al. 2008).

From a theoretical perspective there are multiple candidates for quenching, all of which involve either an active removal of cold gas from a galaxy, or the prevention of gas cooling onto the galaxy. Cold gas may be removed violently during galaxy mergers via a combination of feedback from supernovae, gravitational shocks, and that from an active galactic nucleus (AGN, e.g., Cox et al. 2004; Springel et al. 2005a). The supply of cold gas coming from a hot gas halo may also be shut off by heating from the central AGN (e.g., Croton et al. 2006; McNamara & Nulsen 2007). While these processes are promising, it is not yet clear how well AGNs can efficiently couple to the gas of the galaxy. Alternatively, environmental processes can either strip cold gas as a galaxy falls into a hot intracluster or intragroup medium (ram-pressure stripping; Gunn & Gott 1972) or strip the hot gas halo, thereby depriving the galaxy of fuel for future star formation (strangulation; Larson et al. 1980). These mechanisms for environmental quenching have been incorporated into cosmological simulations by assuming that galaxies have their gas supply cutoff once they enter a larger dark matter halo and become a "subhalo" or "satellite" galaxy. The current (and simple) implementation of this quenching has difficulty in matching the clustering and abundance of red galaxies, implying that the model is too efficient at quenching star formation in low-mass galaxies (e.g., Coil et al. 2008).

Clearly, an important way to constrain the ways in which star formation can be quenched is to study in detail the buildup of the red sequence as a function of galaxy mass or luminosity. For example, it is necessary to understand how the red sequence assembles in regimes where different feedback modes may dominate, e.g., as a function of environment. Clusters of galaxies are one extreme of the dark matter halo power spectrum and are promising test beds for understanding the mechanisms by which star formation can be suppressed. An additional benefit of studying clusters is that the trip to the red sequence in a massive cluster is a one-way street. Cooling of gas from the ambient intracluster medium is likely inefficient and the large relative velocities in massive virialized systems make merging unlikely (but see van Dokkum et al. 1999; Tran et al. 2008, for examples of merging red galaxies in a merging cluster). As we will discuss in this paper, however, galaxy merging may actually have been an important player in early growth phase of clusters.

Measurements of the luminosity function (LF) of red-sequence galaxies in clusters (De Lucia et al. 2004, 2007; Tanaka et al. 2005; Stott et al. 2007; Gilbank et al. 2008; Rudnick et al. 2009) and the field (Rudnick et al. 2009) at $z < 1$ have shown unambiguously that the faint red-sequence population builds up at later times than the bright population. Because light correlates well with mass for red-sequence galaxies, the luminosity trend can also be interpreted as one with stellar mass (although there are potential complications with this simple $M/L$ scaling due to the hierarchical growth of galaxies on the red sequence; Skelton et al. 2012). This late buildup of the faint end therefore implies that whatever quenched star formation may have done so in low-mass galaxies at preferentially later times. By comparing the total luminosities of clusters at $0.4 < z < 0.8$ with their likely descendants at $z \sim 0$ from Sloan Digital Sky Survey (SDSS), Rudnick et al. (2009) found that the total light on the red sequence in clusters must have grown by a factor of one to three over this span of time, similar to the inferred growth of the field red sequence (e.g., Brown et al. 2007).

What is still unknown from an observational standpoint is how the red sequence in clusters evolved at $z > 0.8$. Here, we present a study of the rest-frame $i$-band red sequence and its LF down to faint magnitudes in a $z = 1.62$ cluster XMM-LSS J02182-05102 (also known as IRC0218). This cluster was selected as an overdensity of galaxies with *Spitzer*/IRAC colors indicative of being at high redshift irrespective of their rest-frame colors (Papovich 2008). It was subsequently confirmed using spectroscopy and there are 11 galaxies at $1.62 < z_{\rm spec} < 1.63$ within 1 physical Mpc of the center (Papovich et al. 2010; Tanaka et al. 2010). Its spatial structure implies that it is not relaxed and deep *Chandra* observations have found diffuse emission indicative of a potentially underluminous intracluster medium (Pierre et al. 2012). This galaxy cluster has a strong red sequence (Papovich et al. 2010) despite not being selected on the basis of red rest-frame optical colors. In addition it has a large abundance of star-forming galaxies in the cluster core (Tran et al. 2010).

In this paper, we specifically explore the red-sequence LF and its evolution. In Section 2, we discuss the observations, and the construction of a $K_s$-band-selected catalog. The color–magnitude diagram (CMD) is presented in Section 3. We discuss the future evolutionary path of XMM-LSS J02182-05102 in Section 4. The red-sequence LF is presented in Section 5 along with the evolution of the LF shape and total luminosity of red galaxies in clusters at $z < 1.62$. We discuss our results and the implications for red-sequence growth in Section 6 and conclude in Section 7.

Throughout we assume "concordance" $\Lambda$-dominated cosmology with $\Omega_{\rm M} = 0.3$, $\Omega_\Lambda = 0.7$, and $H_o = 70h_{70}\,{\rm km\,s^{-1}\,Mpc^{-1}}$ unless explicitly stated otherwise. All magnitudes are quoted in the AB system.

## 2. DATA AND OBSERVATIONS

### 2.1. Image Reduction and Calibration

We imaged XMM-LSS J02182-05102 in the $YJK_s$ bands using the HAWK-I instrument (Pirard et al. 2004; Casali et al. 2006) on the Very Large Telescope (VLT) in service mode in the fall of 2010 (PI: Tran; 386.A-0514(A)). Our observations were split up into three Observing Blocks in $Y$, two in $J$, and one in $K_s$. The total integration times were 9360 s, 6240 s, and 3000 s, in $YJK_s$, respectively. The image quality of our observations

was excellent, with FWHM = 0.″52, 0.″60, and 0.″43 in $YJK_s$, respectively.

In order to avoid the gaps between the chips, the cluster was centered in the middle of one of the chips and the field of view was rotated by approximately 45 deg to place other substructures on the centers of different chips. We dithered our observations in pseudorandom pattern within a box 60″ on a side.

The data were reduced using standard techniques for NIR imaging and follow the steps taken for HAWK-I data from Lidman et al. (2008), which include dark subtraction, the application of twilight flats to remove the pixel-to-pixel response, sky subtraction using the XDIMSUM package in IRAF,[6] flux calibration, astrometric calibration, and image combination. SExtractor, SCAMP, and SWarp were used for the astrometric calibration and image combination.[7]

The images were photometrically calibrated using an 8″ diameter aperture on Two Micron All Sky Survey stars within the field for $J$ and $K_s$. The $Y$-band image was calibrated using a UKIRT standard observed on the same night as our observations. The photometric zero points have an uncertainty of 0.02 mag.

### 2.2. Object Detection and Photometry

For the purposes of measuring accurate colors, the $Y$ and $K_s$ images were convolved to the FWHM of the $J$ image, which had the lowest quality. This was done by matching the position of the stellar locus for bright, uncrowded, and unsaturated stars between each of the convolved $Y$ and $K_s$ bands and the $J$ band.

Objects were detected from the native seeing $K_s$-band image using the SExtractor software (v2.5.0). Before detection the $K_s$ image was convolved within SExtractor with a Gaussian having an FWHM = 5.0 pixels, or 0.″53, which corresponds to the point-spread function size. This is applicable for the faintest sources, which are likely unresolved. We experimented with different combinations of the detection threshold (`DETECT_THRESH`) and minimum number of required interconnected pixels (`DETECT_MINAREA`) and decided that the parameters `DETECT_THRESH` = 2.0 and `DETECT_MINAREA` = 1 detected most obvious sources with no clear spurious detections. For the purposes of this paper, spurious sources were identified as faint $K_s$ detections with no counterpart in $Y$ or $J$. We chose `DETECT_MINAREA` = 1 because it can be translated straightforwardly into a magnitude limit for point sources, which simplifies understanding the detection in terms of a total magnitude limit (Labbé et al. 2003). Admittedly, using such a low detection threshold is somewhat ambitious but we wanted to make sure that we went as deep as possible without incurring spurious counts. We therefore tested that most objects near our detection limit had acceptable measurement uncertainties (see below) and that including the faintest objects does not affect our conclusions in any way. We quantify our detection limit below using completeness simulations.

Object photometry was performed in "dual-image" mode, where sources were detected on the unconvolved $K_s$ image and matched aperture photometry was then performed on the seeing-matched images. Following, e.g., Labbé et al. (2003), we chose "color" apertures to maximize the signal-to-noise (S/N) of our colors, while minimizing systematic errors due to crowding. For isolated sources we choose an isophotal aperture unless the isophotal area is less than that of a circle with $d$ = 0.″8. That size corresponds to 1.4× FWHM, which is the size that maximizes the S/N for a Gaussian profile. In the presence of crowding or blending, we choose a $d$ = 1″ circular aperture so that the isophotal aperture size is not corrupted.

Because of correlations in the sky measurements caused by sub-pixel dithering, distortion corrections, and undetected background sources, the measured pixel-to-pixel rms can underestimate the true uncertainty in the flux of an object. Since our objects are much fainter than the sky, the uncertainty in the measured flux is dominated by the uncertainty in the measured value of the sky. Therefore, an appropriate way to estimate the flux uncertainty is to measure the uncertainty in the sky for each flux measurement. We did this using an empty aperture simulations described in, e.g., Labbé et al. (2003). Briefly, for a range of aperture radii we inserted 1000 randomly placed non-overlapping circular apertures into each image, excluding all objects and image boundaries. The distribution of measured fluxes for each empty aperture gives the real uncertainty in the sky measurement. As found by many authors, starting with Labbé et al. (2003), the measured noise scales super-linearly with aperture size and is significantly larger than the expectation from pixel-to-pixel rms assuming pure uncorrelated Gaussian fluctuations. For each object/band/aperture triplet, we computed a linearized aperture size and assigned the appropriate uncertainty as derived from the aperture simulations. Using these simulations, we measured a formal 5$\sigma$ limit for a $d$ = 1″ aperture of 25.2, 24.8, and 24.1 mag in $YJK_s$, respectively, accounting for a point-source aperture correction (see Section 2.2.1).

We require an object to have >50% of the effective exposure time to be included in the analysis. The gaps between the detectors are not excluded by this cut and we therefore only exclude regions around the edges of the image. Twenty-nine percent of the sources in the original catalog were excluded by this cut, but many of the sources with the lowest effective exposure time are likely spurious.

Stars were rejected from the catalog using the SExtractor Stellarity index. We flagged as stars, objects with CLASS_STAR $\geqslant$ 0.99 or those objects with $J - K_s < 0.95$. This cut effectively removed stars on the stellar locus in the $K_s$ versus size plane.

#### 2.2.1. Total Magnitudes

We measure total magnitudes in the $K_s$ image using the SExtractor AUTO magnitude with a point-source aperture correction. The AUTO aperture scales with the first moment of the object radial flux profile. While a floor on the size of the AUTO aperture was set, for small (and usually faint) objects it is nonetheless the case that significant flux can be missed by the small AUTO aperture. We compute a minimal aperture correction for point sources using the methodology described in Labbé et al. (2003) and Rudnick et al. (2009).

We found seven bright isolated stars in our $K_s$ image and calculated each of their curves of growth (COG), which were normalized at $r$ = 4″, corresponding to the aperture used for our zero-point determination. These were then averaged to obtain an average curve of growth for stars in the image. For each object the aperture correction was computed from the COG using the circularized AUTO aperture radius. For our faintest objects ($23 < K_s(\mathrm{AUTO}) < 23.5$), the mean aperture correction is 0.15 mag with an rms of 0.04 mag. This point-source correction can be regarded as the minimal correction to an object's total flux. While this correction undoubtedly misses some flux for extended objects, it must be applied for all objects and is likely

[6] IRAF is distributed by the National Optical Astronomy Observatories which are operated by the Association for Research in Astronomy, Inc., under the cooperative agreement with the National Science Foundation.

[7] Available at http://terapix.iap.fr.

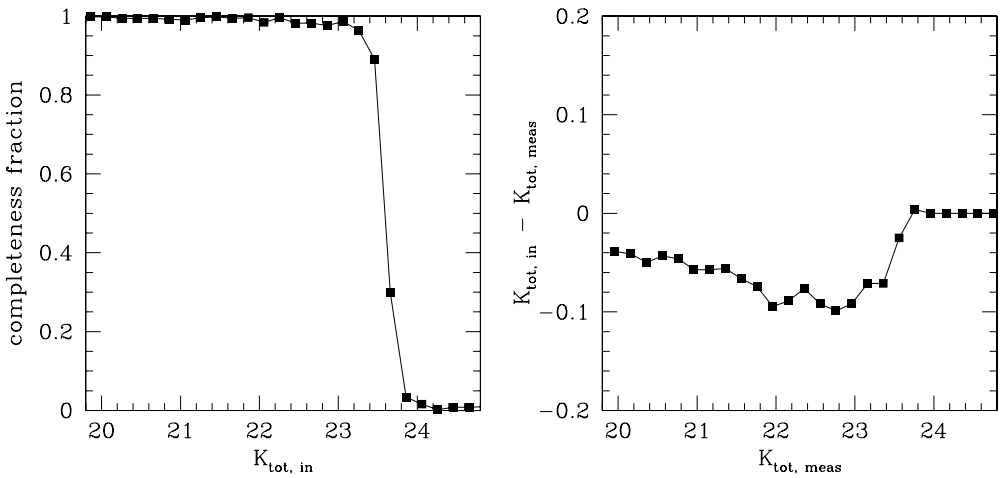


**Figure 1.** Results of our point-source completeness simulation. Left panel: the completeness fraction, defined as the ratio of detected sources over input sources, as a function of input magnitude. The completeness drops precipitously at $K_s > 23.4$ mag. Right panel: the error in total magnitude (including point-source aperture correction) as a function of measured magnitude. The error in total magnitude for faint resolved sources is less than 0.1 mag.

appropriate for faint sources near the resolution limit. Robust modeling of the aperture correction for the brighter and more extended sources is difficult as we do not have an accurate measure of their profile shape. For the rest of the paper, all of our $K_s$ magnitudes include this aperture correction.

#### 2.2.2. Catalog Completeness

To assess our catalog completeness, we performed a simulation to determine how well we detect point sources, which should be good analogs for the nearly unresolved objects near our detection limit. We added 500 sources to the native seeing $K_s$ image, in batches of 100 to maintain the intrinsic crowding of the images, and detected the objects with the same parameters used on the science data. We then measured the error in the magnitude as a function of measured magnitude and the fraction of recovered sources as a function of input magnitude. The results of these simulations are shown in Figure 1. Our 90% completeness limit is $K_s = 23.4$ and the amount of flux that we miss with our total magnitude estimate (including aperture correction) is less than 0.1 mag for objects brighter than this. The 90% completeness limit corresponds almost exactly to the formal $5\sigma$ limit determined from our aperture simulations. It is also the magnitude at which the numbers of observed galaxies start to rapidly fall (see Figure 2), just as expected from our completeness simulation, where the completeness falls from 90% to 30% in just 0.2 mag. This rapid decline in completeness is a direct result of our aperture corrections, as has been seen in other works (e.g., Labbé et al. 2003; White et al. 2005).

## 3. THE COLOR–MAGNITUDE DIAGRAM

The $K_s$ versus $Y-J$ CMD for all galaxies within 2 arcmin (1 Mpc) of the cluster center is shown in the left panel of Figure 2. At $z = 1.62$ $Y-J$ corresponds to the age-sensitive $U-B$ rest-frame color as the $Y$ and $J$ filters straddle the 4000 Å break. The $K_s$ magnitude is very close to the rest-frame $i$ band. The plotted CMD includes the contribution of all galaxies along the line of sight. In constructing the LF, we will statistically subtract the field to measure the LF of the members but here discuss the full CMD. Even from this, however, there are several items worth commenting on.

There is a clear red sequence that is well separated from the blue star-forming galaxies, as found in Papovich et al. (2010) and Tanaka et al. (2010) using significantly shallower data. Papovich et al. (2010) demonstrated that the brightest red-sequence galaxies have rest-frame $U-B$ colors and a color scatter consistent with a formation redshift of $2.35 \pm 0.1$, indicating that they experienced their last major episode of star formation $1.2 \pm 0.1$ Gyr before being observed.

It is possible that some of the galaxies on the red sequence have colors dominated by dust extinction since some of them have 24 $\mu$m emission consistent with obscured star formation, or possibly an AGN (Tran et al. 2010). Yet, >80% of the bright red-sequence galaxies have SED fits to their rest-frame $0.15\,\mu\text{m} < \lambda < 3.0\,\mu\text{m}$ which do not indicate significant amounts of dust extinction (Tran et al. 2010; Papovich et al. 2012; Lotz et al. 2011). Also, some of the spectroscopic members are on the red sequence and a significant fraction of these objects do not show evidence of emission lines in their spectra (Tanaka et al. 2010), although emission lines should have been detectable at the cluster redshift (Papovich et al. 2010).

We determine the slope and zero point of the red sequence by using a robust line-fitting algorithm on all galaxies with $Y - J > 0.6$ that have errors in $Y-K$ and $K_s$ less than 0.2 mag. The slope and color at $K_s = 20$ are $-0.03 \pm 0.03$ and $0.95 \pm 0.13$.[8] The zeropoint of the CMD is completely consistent with a predicted $Y - J$ color of 0.94 for a single-age population formed at $z = 2.35$ as found in Papovich et al. (2010).

We find a striking lack of red galaxies at faint magnitudes. This is reminiscent of the lack of faint red galaxies in clusters at $z < 1$ (De Lucia et al. 2004, 2007; Tanaka et al. 2005; Stott et al. 2007; Gilbank et al. 2008; Rudnick et al. 2009) and in a $z = 1.46$ cluster (Hilton et al. 2009), but now seen in a $z = 1.62$ cluster. It is worth addressing possible explanations for this deficit. This effect is not due to detection incompleteness as we detect blue galaxies down to the 90% completeness limit. The completeness could be a function of color if the faint red galaxies have a larger size than blue galaxies at the same total magnitude but we find this to be an unlikely possibility given the smaller size of faint red galaxies at these redshifts compared with blue galaxies (e.g., Zirm et al. 2007; Toft et al. 2007).

[8] The line fit remains unchanged if we include all galaxies with $Y - J > 0.6$ and the resultant red-sequence LF remains unchanged if we assume a constant color with magnitude for the red sequence.

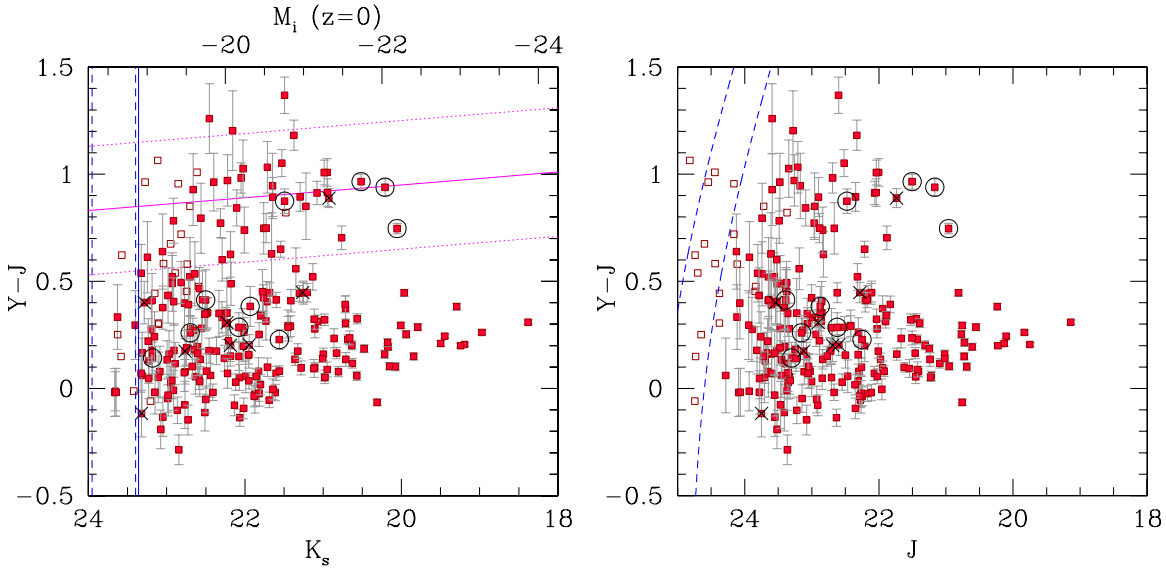


**Figure 2.** Observed color–magnitude diagrams for all of the objects within 2 arcmin (1 Mpc) of the cluster center. The catalog is selected in the $K_s$ band and the $J$- and $Y$-band data are 0.7 and 1.0 mag deeper than $K_s$, respectively. The open circles and crosses mark spectroscopically confirmed members and non-members, respectively. Left panel: the vertical blue solid line is the 90% detection completeness limit and the vertical dashed blue lines correspond to the formal $5\sigma$ and $3\sigma$ limits in a $d = 2''$ circular aperture. There is no unique relation between our $K_s$-band limit and a limit in $Y-J$ color, but in both panels we use open squares to show those objects with a $Y-J$ color uncertainty greater than 0.2 mag (see the right panel). The solid magenta line is a fit to all the galaxies with $Y-J > 0.6$ and the dotted lines indicate $\pm 0.3$ mag around this line. The labels on the top of the figure indicate the absolute $i$-band magnitude derived from passively evolving the red sequence by 1.94 mag from $z = 1.62$ to $z = 0$. This can be directly compared with the magnitude in Figure 4 and is only valid for red-sequence galaxies. Right panel: here the curved dashed lines indicate the reddest colors for which we can achieve a $3\sigma$ and $5\sigma$ measurement on the color in a $d = 0.''8$ circular aperture, which is appropriate for objects near our detection limit. As is evident from these plots, the apparent lack of red objects at faint magnitudes is real and does not stem from either detection incompleteness or from an inability to measure accurate colors.

To assess the effect of color uncertainties on the perceived deficit of faint red galaxies we plot the $Y-J$ versus $J$ CMD in the right panel of Figure 2. In this plot, the curved lines represent the reddest color to which we can measure the $Y-J$ color at the $3\sigma$ and $5\sigma$ level in an aperture of a size appropriate for objects close to our detection limit. It is important to note that this line is not a completeness limit but rather the limit to which colors can accurately be determined. The apparent lack of objects at magnitudes slightly brighter than the $5\sigma$ line reflects our $K_s$-band detection limit and the fact that our $J$- and $Y$-band data are 0.7 and 1.0 mag deeper than $K_s$, respectively. The open symbols in both panels are the same objects and correspond to those with color errors in excess of 0.2 mag. It is clear from this plot that the apparent lack of objects at the faint end of the red sequence is neither an issue of incompleteness nor does it result from large color errors, as we could have measured colors accurately for objects in the empty faint region of the red sequence if they were there.

It is important to realize that this deficit is robust to considerations of cluster membership as we plot all galaxies within a projected distance of 1 Mpc from the cluster. Finally, it is possible that galaxies with large color errors may be preferentially scattered off the red sequence. As we will discuss in Section 5, when performing the membership determination using statistical background subtraction, assuming all of the galaxies with large errors lie on the red sequence does not remove the presence of an observed deficit. Therefore, the lack of observed faint red galaxies implies that these galaxies are not present at any redshift.

## 4. THE FUTURE GROWTH OF XMM-LSS J02182-05102

To place XMM-LSS J02182-05102 into an evolutionary context, we must identify its likely descendants at lower redshift. To do this we must therefore understand its expected growth in a hierarchically evolving universe. There are two mass measurements of XMM-LSS J02182-05102. The first is derived from the X-ray luminosity using the local luminosity–temperature and temperature–mass relations, which yields $M \sim (7.7 \pm 3.8) \times 10^{13}\ M_\odot$ (Pierre et al. 2012).[9] The second is derived from the velocity dispersion of the galaxies and is $M \sim 4 \times 10^{14}\ M_\odot$ (Papovich et al. 2010). As shown in the Appendix, both mass estimates are entirely consistent with that based on the total red-sequence light as calibrated from lower redshift measurements. Given the large degree of substructure, this cluster is likely unrelaxed and we adopt the X-ray mass for the rest of the paper. We predict the mass growth of XMM-LSS J02182-05102 using the halo growth histories of Wechsler et al. (2002), which in turn uses the distribution of halo concentrations from Bullock et al. (2001) for a halo at this mass and at this redshift. Poggianti et al. (2006) showed that these results match the predictions from the Millennium simulation (Springel et al. 2005b). In Figure 3, we show this growth and compare it to the masses of SDSS and EDisCS clusters as derived from their galaxy velocity dispersions (Milvang-Jensen et al. 2008). It is clear that XMM-LSS J02182-05102 will evolve into a typical ($\log(M/M_\odot) \sim 14.3$–15) system by $z < 1$ even taking into account the dispersion in merger histories of such massive halos. We will use this projected growth in subsequent sections when studying the evolution of the galaxies in XMM-LSS J02182-05102.[10]

[9] The X-ray luminosity for this cluster is not given in Pierre et al. (2012).

[10] Had we adopted the mass from the galaxy velocity dispersion, the predicted descendants of XMM-LSS J02182-05102 would have been among the more massive clusters in the universe at any redshift. Such a massive nature for XMM-LSS J02182-05102 may be unlikely given how rare such objects are. Also, it is worth noting that the mass function of clusters at any epoch is very steep and that low-mass descendants will be preferred over high-mass ones. Therefore, in addition to more precise mass measurements, a more careful treatment of the cluster mass function would be required to obtain a more accurate estimate of the typical descendant at each redshift.

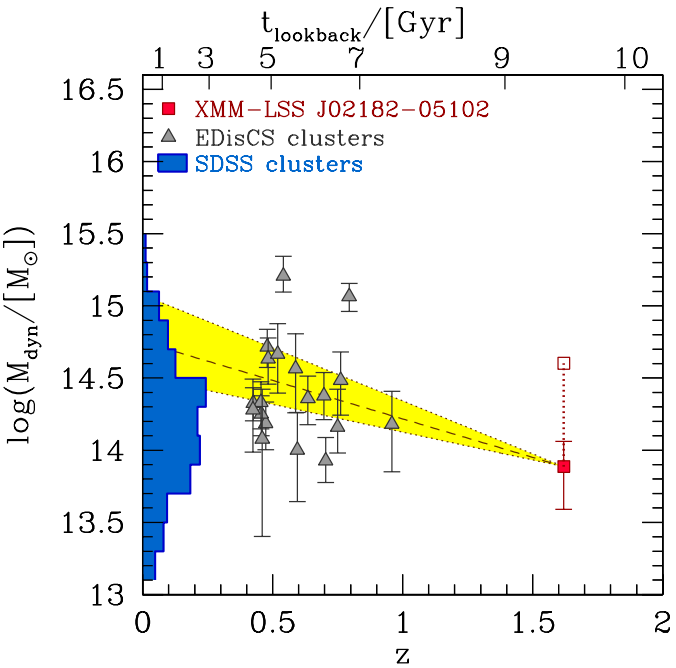


**Figure 3.** Expected growth in mass of XMM-LSS J02182-05102 to $z = 0$. The red solid square represents the X-ray-derived mass for XMM-LSS J02182-05102 (Pierre et al. 2012). The open square connected to the solid by a dotted line indicates the dynamical mass estimate from Papovich et al. (2010), which is significantly higher than the X-ray mass. The disagreement between the two likely masses reflects the unrelaxed dynamical state of the system. The gray triangles represent the EDisCS clusters. The shaded histogram represents the distribution of dynamical masses from our local SDSS sample. The diagonal dashed line gives the median-expected growth in mass for XMM-LSS J02182-05102 from the halo growth histories of Wechsler et al. (2002) and using the halo concentrations of Bullock et al. (2001). The dotted lines and yellow shaded region give the 68% confidence limits on the growth given by the range in the halo concentrations for a cluster of this mass observed at $z = 1.62$. The likely descendants of XMM-LSS J02182-05102 will be fairly typical clusters at all redshifts.

## 5. THE RED-SEQUENCE LUMINOSITY FUNCTION

### 5.1. Cluster Membership

As very few spectroscopic redshifts are available in the core of the cluster, and most of them are for blue galaxies, we identify which galaxies are red-sequence members using a statistical subtraction technique. Rudnick et al. (2009) demonstrated that using statistical background subtraction to isolate red-sequence members in clusters at $0.4 < z < 0.8$ yielded results that were identical to those computed using accurate photometric redshifts. An advantage of statistical background subtraction for membership of faint galaxies is that photometric redshift-based membership techniques often rely on integrating the redshift probability distribution ($P(z)$). Faint galaxies will have lower photometric S/N and hence broader $P(z)$, and the traditional method of establishing a threshold in the integrated probability (Brunner & Lubin 2000) will more likely reject these objects, which is undesirable given the goals of this paper. On the other hand, statistical background subtraction does not have a formal dependence on the S/N, other than being optimal when the distribution of color and magnitude errors of the field and cluster samples are identical, which is the case for our analysis.

Based on our experience (Rudnick et al. 2009) a suitable background subtraction field needs to have comparable band-passes (for red-sequence selection), depth, and total magnitude measurements to the main survey field. A wide area is also desirable. We searched the literature for data that satisfy these requirements but have not found them. For example, UKIDSS and GOODS, while deep and wide, do not include $Y$-band data at our depth. We therefore decide to use the outskirts of our HAWK-I image to define the background population. While it is possible that the outskirts of our image may contain the imprint of the associated large-scale structure, it may indeed be correct to subtract this "local" field rather than a field drawn from a cosmic average.

**Table 1**
Rest-frame $i$-band Luminosity Function of XMM-LSS J02182-05102

| $M_{i,\mathrm{bright}}$ | $M_{i,\mathrm{faint}}$ | $\Phi$ | $\delta\Phi_-$ | $\delta\Phi_+$ |
|---|---|---|---|---|
| −24.5 | −24.0 | 1.0 | 0.83 | 2.41 |
| −24.0 | −23.5 | 0.85 | 0.85 | 2.36 |
| −23.5 | −23.0 | 5.08 | 2.17 | 3.47 |
| −23.0 | −22.5 | 5.85 | 2.34 | 3.62 |
| −22.5 | −22.0 | 2.79 | 1.56 | 2.94 |
| −22.0 | −21.5 | 0 | 0 | 2.0 |
| −21.5 | −21.0 | 2.19 | 1.36 | 2.78 |
| −21.0 | −20.5 | 0.54 | 0.54 | 2.24 |

**Notes.** $\Phi$ corresponds to the number of galaxies in the magnitude range specified with no evolution corrections applied. The non-integer values are a byproduct of our statistical background subtraction technique. The last two columns are the positive and negative uncertainty in this number as determined from Poisson uncertainty on the counts. There is one mag bin with no galaxies detected.

For the purposes of the subtraction, we define two regions, the cluster at $r_{\mathrm{proj}} < 0.75$ Mpc[11] and the field at $r_{\mathrm{proj}} > 1.5$ Mpc. After selecting galaxies within $\pm 0.3$ mag of the red sequence, we bin the observed $K_s$-band magnitudes in both regions and then subtract the field histogram from the cluster histogram, normalizing the field histogram by the ratio of the field area to the cluster area. This results in an observed $K_s$ LF for likely red-sequence cluster members.

### 5.2. The Luminosity Function

We construct the LF in the rest-frame $i$ band for comparison with lower redshift studies (e.g., Rudnick et al. 2009). To do this we take advantage of the fact that the $K_s$ band is very close to the redshifted rest-frame $i$-band filter. Using the technique described in Rudnick et al. (2003) to compute $i_{\mathrm{rest}}$ we find that the $k$-corrections for red-sequence galaxies at the cluster redshift are consistent with a constant $m_{K_s} - M_i = 44.13$ with a 0.03 mag dispersion. We apply this correction to the observed LF to obtain a rest-frame $i_{\mathrm{rest}}$-band LF for red-sequence cluster members.

The shape of this LF is insensitive to the exact slope of the red sequence and the width of our red-sequence cut. We also test how the LF would change if we assumed that all galaxies with $Y - J$ errors more than 0.2 mag were all on the red sequence. Since this adds similar numbers of galaxies to the field and cluster CMDs, the shape of the subtracted cluster LF is unchanged.

In Table 1, we give the red-sequence LF of XMM-LSS J02182-05102 and show it in Figure 4 compared to the composite red-sequence LF in clusters at $z = 0$, $z = 0.5$, and $z = 0.7$ from Rudnick et al. (2009). As we will discuss shortly, there is clearly strong evolution in the shape of the LF at $z < 0.7$, with little shape evolution from $z = 1.62$ to $z = 0.7$.

In Section 4, we showed that XMM-LSS J02182-05102 is likely the progenitor of "typical" clusters in EDisCS and SDSS

[11] This is chosen to match the aperture used for the lower redshift comparison samples. Its exact value does not affect our conclusions.

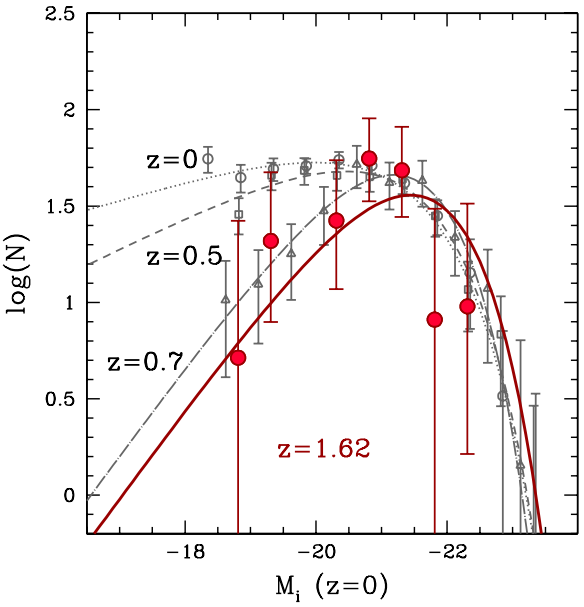


**Figure 4.** Rest-frame *i*-band luminosity function for the cluster XMM-LSS J02182-05102 at $z < 1.62$ is shown as the solid red circles. Magnitude bins with no objects are not plotted. The gray open circles, squares, and triangle symbols are the LFs for composites of clusters at $z < 0.06$, $0.4 < z < 0.6$, and $0.6 < z < 0.8$, respectively, from Rudnick et al. (2009). The error bars are Poisson errors only. The dotted, dashed, and dot-dashed lines are the Schechter (1976) fits to the $z < 0.8$ clusters with $\alpha$ left as a free parameter. The solid line is the fit to the $z = 1.62$ cluster with $\alpha$ left fixed to the $z = 0.7$ value. The magnitudes shown here have all been passively evolved to $z = 0$ as described in the text. The LFs have also been scaled vertically to have the same integrated luminosity. The measured LF at $z = 1.62$ is similar in shape to that at $z = 0.7$ and shows a significant decline toward fainter magnitudes and a lack of bright galaxies.

and so in Figure 4 we therefore compare the XMM-LSS J02182-05102 LF to the total composites for these two lower redshift samples. In Figure 4, we have faded all the LFs to $z = 0$ assuming that the red-sequence galaxies all formed at $z = 2.35$ and evolved passively thereafter. As has been seen before, the red-sequence LF evolves strongly in shape at $z < 0.8$ with the faint galaxy population building up progressively toward lower redshift (De Lucia et al. 2004, 2007; Tanaka et al. 2005; Stott et al. 2007; Gilbank et al. 2008; Rudnick et al. 2009). This has been associated with the late addition of faint galaxies to the red sequence.

The assumed fading is consistent with the evolution in the mean color and color scatter of the red sequence in this and other clusters (Papovich et al. 2010). Whitaker et al. (2010) found that passive galaxies at $z \sim 1.6$ have a spread in their ages of about 1 Gyr but this would result in a spread in the measured fading to $z = 0$ of 0.6 mag and should not affect our results. The spread in fading is even less if the galaxies are only faded to $z = 0.7$ as we do in Section 5.3.

Given this strong evolution at $z < 0.8$, it is striking that the observed LF at $z = 1.62$ is remarkably similar in shape to that $z = 0.7$, with the same turnover toward faint magnitudes. At the same time, the bright end of the LF at $z = 1.62$ appears to be underpopulated with respect to the individual lower redshift clusters (see individual cluster LFs from Rudnick et al. 2009). This is similar to what has been found in a $z = 1.46$ cluster (Hilton et al. 2009). Taken together this implies that galaxies must be added to the bright end between $z = 1.62$ and $z = 0.7$ but that the shape of the LF should remain relatively constant. In the following section, we will discuss possible scenarios for the evolution of the LF and how it relates to the evolution of the cluster red sequence.

The Schechter (1976) function fits to the EDisCS and SDSS LFs were presented in Rudnick et al. (2009) and were computed with $\alpha$, $M^\star$, and the normalization as free parameters. Our LF at $z = 1.62$ does not have enough S/N to allow a simultaneous determination of $\alpha$ and $M^\star$ but we attempted to constrain $M^\star$ by fixing $\alpha = 0.17$ as determined from the $z = 0.7$ clusters. While the lack of bright galaxies allowed no strong constraints to be placed on $M^\star$, the best-fit Schechter function with a fixed $\alpha = 0.17$ (Figure 4) is a statistically acceptable fit to the observe LF.

Tanaka et al. (2010) showed that the red-sequence LF of XMM-LSS J02182-05102 as derived from significantly shallower NIR data appeared similar to that from groups at $z = 1.1$ from Tanaka et al. (2008), which in turn had a deficit of faint galaxies. At the same time, the very massive $z = 1.1$ cluster from Tanaka et al. (2008) had a red-sequence LF that appeared similar to that from SDSS clusters, but was very different from that for XMM-LSS J02182-05102. The strong cluster mass dependence of the LF contrasts with the result from Rudnick et al. (2009), who found only a very weak dependence of red-sequence LF shape on cluster mass. Indeed, the LF for the most massive cluster from EDisCS in its high-redshift sample (CL1216.8-1201, $z = 0.8$) is consistent with both the $z = 0.7$ EDisCS composite LF and that for XMM-LSS J02182-05102 but inconsistent with the $z = 0.5$ EDisCS composite. As noted in Tanaka et al. (2008) and Rudnick et al. (2009), this apparent discrepancy may result from the large cluster-to-cluster variance in galaxy properties at a fixed mass. Clearly larger samples of well-studied clusters are needed at $z > 0.5$ over a range of cluster mass.

### 5.3. The Integrated Luminosity of the Red Sequence

In addition to determining the evolution (or lack thereof) in the shape of the LF, a complete description of the growth of the red sequence also requires a measurement of how the total red-sequence light in clusters increases over time. To do this, we integrate the observed red-sequence LF for XMM-LSS J02182-05102 ($L_{\rm tot,RS}$) and compare it to that for clusters at $0.4 < z < 0.8$ from EDisCS and at $z = 0$ from SDSS. The results are shown in Figure 5. Our LF depths at all redshifts have been constructed to have identical faint limits when corrected for passive luminosity evolution—indeed this drove our HAWK-I exposure times. For that reason, integrating the observed LFs yields an $L_{\rm tot,RS}$ measurement that extends to a roughly constant stellar mass limit.

It is important to compare this cluster with its likely descendants at low redshift as the most massive clusters also have the red sequences with the highest $L_{\rm tot,RS}$ (see the Appendix). As described in Section 4 and as shown in Figure 3 the most likely descendants of XMM-LSS J02182-05102 are typical clusters at $z < 1$ with $\log(M/M_\odot) \sim 14.3$–15. In Figure 5, we have highlighted which of the EDisCS clusters are the likely descendants based on the projected mass evolution.

We compare our clusters within a constant physical aperture of $r = 0.75$ Mpc. This does not take into account that clusters may preferentially grow from the inside out (e.g., Balogh et al. 2000). On the other hand, given the very uncertain mass of XMM-LSS J02182-05102 and the poor mass determination of some of our SDSS clusters—due to a small number of available spectroscopic redshifts—using a constant metric aperture is more robust than one that scales as mass, e.g., $R_{200}$.

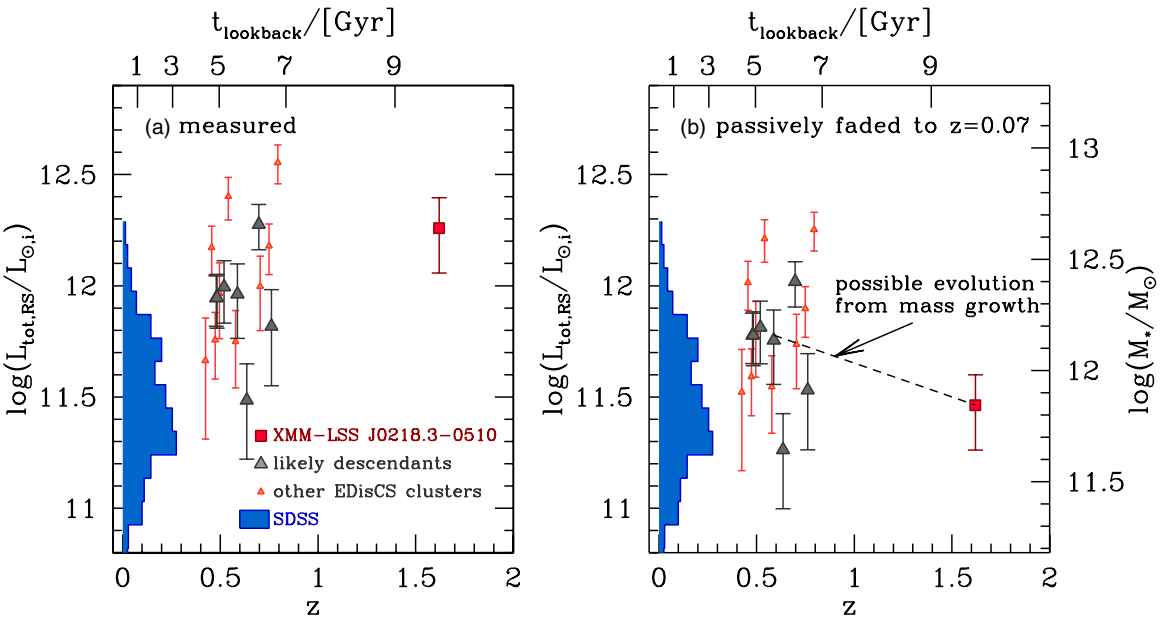


**Figure 5.** Total amount of light on the red sequence, $L_{\rm tot,RS}$, in clusters at $z < 1.62$. The shaded histogram represents the distribution total red-sequence luminosities from our local SDSS sample. In both panels, the triangles indicate the EDisCS clusters, with the larger triangles showing those clusters that are the likely intermediate-redshift descendants of XMM-LSS J02182-05102 based on the likely mass growth from Figure 3. The error bars on the EDisCS and XMM-LSS J02182-05102 point account for the statistical errors in the individual cluster LF determinations. Left panel: $L_{\rm tot,RS}$, computed by integrating the measured red-sequence luminosity functions. Right panel: both the EDisCS clusters and XMM-LSS J02182-05102 have had their $L_{\rm tot,RS}$ adjusted by fading the light on the red sequence to $z \sim 0$ by an amount expected for a simple stellar population with $z_{\rm form} = 2.35$. Using this $M/L$ correction, we plot the total stellar mass of red sequence cluster galaxies as predicted at $z = 0$ on the $y$-axis. The dashed line is a least-squares fit to the $L_{\rm tot,RS}$ values for XMM-LSS J02182-05102 and its likely intermediate-redshift descendants.

In the left panel of Figure 5, it is clear that the $L_{\rm tot,RS}$ of the most luminous cluster red sequences at $z < 1.62$ is comparable to within a few tenths of a dex. However, we must account for the expected fading of the stellar populations in the red-sequence galaxies as they age. To this end, we fade all of the cluster red sequences to $z = 0$ using a simple stellar population formed at $z = 2.35$, which is consistent with the color evolution of the bright red-sequence galaxies over this whole redshift range (Papovich et al. 2010). The faded total luminosities are shown in the right panel of Figure 5. Under the assumption that all the red-sequence galaxies at all redshifts have the same star formation history (SFH), this roughly converts $L_{\rm tot,RS}$ into a stellar mass content on the red sequence.[12] We speculate on the evolution of XMM-LSS J02182-05102, by performing a least-squares fit to the $L_{\rm tot,RS}$ values for XMM-LSS J02182-05102 and the likely descendants among the EDisCS clusters. This is shown as the dashed line in the right panel of Figure 5.

Given the likely evolutionary path, the red sequence in XMM-LSS J02182-05102 grew by a factor of $\sim$2 in light or stellar mass during the $\approx$4 Gyr between $z = 1.62$ and $z = 0.6$. In Section 6, we will discuss how to reconcile this rapid growth in the luminosity with the lack of shape evolution between $z = 1.62$ and $z = 0.7$. Assuming that the evolutionary path in Figure 5 continues to $z = 0$ then the cluster will grow by an addition 50% between $z = 0.6$ and $z = 0$ or a factor of three in total since $z = 1.62$.

As a cautionary note, given the rapid evolution in the shape of the LF at $z < 0.6$, it is likely incorrect to assume a constant amount of fading for all galaxies, as those added more recently to the red sequence will fade more rapidly with time. To approximate this effect, we varied the amount of fading assuming a $z_{\rm form}$ for XMM-LSS J02182-05102 ranging from $z = 2$ to 3 and for the EDisCS clusters ranging from $z = 1$ to 2. While the exact trend of $L_{\rm tot,RS}$ with $z$ depends on the exact mix of $z_{\rm form}$, the change in maximum growth in $L_{\rm tot,RS}$ was $\sim$0.1 dex over the full redshift range.

[12] Skelton et al. (2012) have pointed out that this assumption may be inappropriate given the hierarchical buildup of red-sequence galaxies but we assume it here for simplicity.

## 6. DISCUSSION

Our first result, that there is a deficit of faint red galaxies in XMM-LSS J02182-05102, may result naturally from a scenario in which galaxy star formation is quenched once a galaxy's total mass moves above $10^{12}\,M_\odot$ and it forms a hot gas halo. This naturally predicts that the most massive galaxies are quenched first and that there should be relatively few low-mass passive galaxies at high redshift (Gabor & Davé 2012).

In explaining our other findings on the growth of the red sequence over time we must explain some apparently contradictory results. First, we find that the LF of red-sequence galaxies in clusters evolves very little *in shape* from $z = 1.62$ to $z = 0.6$. At redshifts lower than this, however, the shape evolves rapidly, such that the faint-end slope becomes shallower, eventually matching the $z = 0$ value (Figure 4). At the same time, Figure 5 alone implies that the total stellar mass on the red sequence appears to increase by a factor of $\sim$2 during the $\sim$4 Gyr from $z = 1.62$ to $z = 0.6$ and then grows by only 50% over the remaining $\sim$6 Gyr to the present day. In Rudnick et al. (2009), it was shown that adding the minimal possible number of galaxies to the red sequence at $z < 0.8$ would actually cause the predicted $L_{\rm tot,RS}$ in SDSS clusters to be too high. Resolving this discrepancy can be accomplished by assuming that a significant fraction of the stars in galaxies that are added to the red sequence at $z < 0.8$ end up as intracluster stars. At $z > 0.7$, we appear to have the opposite problem. The total light in the clusters must grow rapidly, but without changing the shape.

At first glance, resolving this problem is difficult. There are no blue galaxies in the field at this redshift luminous enough to fade onto the bright end of the red sequence in this cluster (Papovich et al. 2010), which implies that most of the mass must be added in the form of fainter galaxies. However, this would result in a shape change of the LF that is not seen between $z = 1.62$ and $z = 0.7$. A hint perhaps lies in the lack of red galaxies in XMM-LSS J02182-05102 brighter than $M_i = -24.2$, or $M_{i,\mathrm{fade}} = -22.25$, as has also been seen in Hilton et al. (2009). This is in contrast to the individual EDisCS clusters, which are populated with galaxies to at least 0.5 mag brighter than this, when accounting for the passive fading of the stellar populations (see individual LFs from Rudnick et al. 2009). Therefore, despite the lack of blue luminous galaxies that could fade onto the red sequence, the bright red-sequence population must grow between $z = 1.62$ and 0.7. One solution to this problem is for galaxies in the blue cloud at fainter magnitudes ($\sim L^\star$) to rapidly form stars and then be quenched, all on short enough timescales to prevent them from showing up in the observed population. The amount of stars that need to be formed in such an episode, however, would require SFRs much in excess of what is measured for galaxies in this field at $z \sim 1.6$ from MIPS 24 $\mu$m data (Tran et al. 2010).

### 6.1. The Importance of Mergers

A more likely explanation is that the fainter blue galaxies fall into the cluster, have their star formation suppressed somewhere during the process (in groups or the cluster itself), and migrate to the faint end of the red sequence, where they subsequently merge with other red-sequence galaxies and increase their mass. It is reasonable that the SFRs of infalling galaxies are suppressed as they fall into the cluster environment, via ram-pressure stripping (Gunn & Gott 1972) or galaxy strangulation (Larson et al. 1980). Indeed Pierre et al. (2012) have found that XMM-LSS J02182-05102 has a diffuse X-ray component indicating the presence of a heated (but possibly underluminous) intergalactic medium. Such a scenario would have the effect of offsetting the addition of galaxies to the red sequence at faint magnitudes by merging them up the red sequence and hence preserving the shape of the LF, while at the same time allowing the cluster to grow its total red-sequence stellar mass to agree with the likely descendant clusters in the EDisCS sample.

To test this we perform a simulation where we add galaxies to the red sequence between $z = 1.62$ and $z = 0.6$ and then test how the resultant red-sequence LF shape and normalization depends on the different number of mergers per galaxy. Because the shape and normalization are important for this test, we compare the LF for XMM-LSS J02182-05102 to the composite EDisCS LF normalized to the mean $L_{\mathrm{tot,RS}}$ of the likely descendant clusters.

We assume that infalling field galaxies have a constant SFR until a time $t_{\mathrm{cut}}$ before they are rapidly quenched. This quenching happens a time $t_{\mathrm{delay}}$ before they are added to the cluster. This insures that they are red by the time they enter the cluster. During the quenching process they lose $A_i$ magnitudes of internal extinction. For the purpose of this test, we choose $t_{\mathrm{cut}} = 3$ Gyr, $t_{\mathrm{delay}} = 1.0$ Gyr, and $A_i = 0.7$ mag (corresponding to $A_V = 1$ for a Calzetti et al. 2000 attenuation curve), although we note that our results are not sensitive to the exact values adopted (see below). This scenario assumes that the SFRs of galaxies are suppressed before falling into the cluster environment, and that in the transformation to red-sequence galaxies they lose some amount of dust extinction. This general scenario is consistent with previous works (e.g., Poggianti et al. 2006; De Lucia et al. 2007; Rudnick et al. 2009; McGee et al. 2011) and results in galaxies with colors on the red sequence by $z = 0.6$.

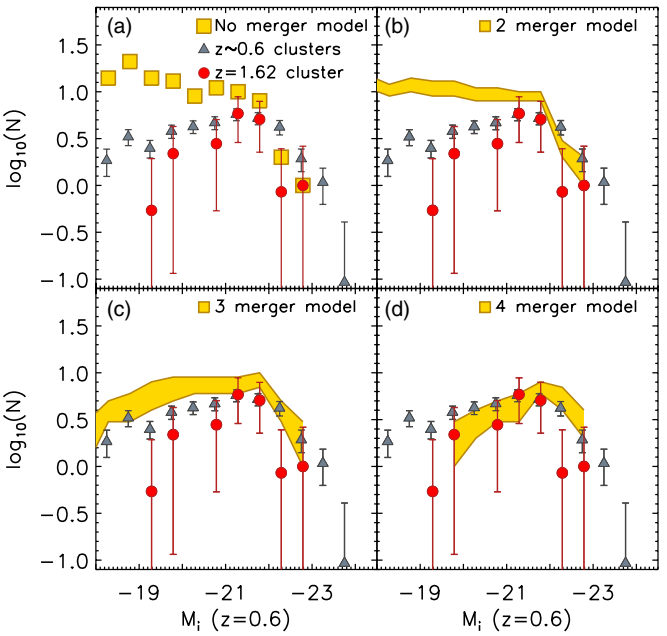


**Figure 6.** Demonstration of how merging and accretion will affect the evolution in the red-sequence LF between $z = 1.62$ and $z = 0.6$. In all panels the vertical scaling of the luminosity functions is accurate in an absolute sense. The $x$-axis refers to the magnitude that galaxies are predicted to have at $z = 0.6$ assuming the SFHs given in the text. The red circles show the LF of XMM-LSS J02182-05102. The gray triangles show the composite EDisCS red-sequence LF scaled in luminosity to the mean $L_{\mathrm{tot,RS}}$ of the likely descendant clusters at $z = 0.6$. These points are the same in each panel. The panels show a set of model predictions for the LF at $z = 0.6$ that assume that the cluster accretes enough recently quenched galaxies to account for the evolution in total red-sequence light at $M_i(z = 0.6) < -19$. The squares in panel (a) show the predicted LF in the absence of merging of passive galaxies. The filled bands in panels (b), (c), and (d), represent how the predicted LF will change if every passive galaxy randomly merges two, three, or four times between $z = 1.62$ and $z = 0.6$. The extent of the bands corresponds to the 25% and 75% confidence intervals on the predicted LF resulting from a Monte Carlo simulation as described in the text. The extent of the bands in magnitude corresponds to where the simulated LFs contain a median of one galaxy. The cluster LF shape and normalization at $z = 0.6$ can be approximately reproduced if every galaxy merges approximately three to four times over the intervening ~4 Gyr between $z = 1.62$ and $z = 0.6$.

Over the 3.8 Gyr between $z = 1.62$ and 0.6, the cluster red sequence of XMM-LSS J02182-05102 has to increase its total stellar mass by a factor of two to match $L_{\mathrm{tot,RS}}$ for the likely descendants at $z \sim 0.6$. We split the necessary mass increase equally between three identical intervals of time over this redshift range. In each interval, we draw galaxies from the evolving blue field galaxy LF from Salimbeni et al. (2008) and evolve them using the SFH parameters above to predict their luminosities at $z = 0.6$. The Salimbeni LF is computed in the rest-frame $B$ band. We convert it to the rest-frame $i$ band assuming a constant SFH with 1 mag of extinction. The result of this process is shown in Figure 6(a) as the yellow squares, which are compared to the XMM-LSS J02182-05102 and EDisCS LF. There we can see that such a scenario of simply accreting and quenching galaxies from the star-forming field population to make up the observed total luminosity increase would produce a faint-end slope much steeper than what is observed in clusters at $z = 0.6$.

We then merge each galaxy with a random second galaxy and perform this up to four times. We perform 100 Monte Carlo

iterations of these mergers and show the 25% and 75% limits of the distribution of the resultant LF as the yellow bands in Figures 6(b)–(d) for two, three, and four mergers per galaxy, respectively. It appears that merging each red-sequence galaxy three to four times with another red-sequence galaxy results in an LF that is similar to that observed at $z = 0.6$. This implies a merger rate of $\sim$1 per Gyr over this time period, integrated over all merger mass ratios. The faint-end slope for this model has the necessary turnover but the bright end is still underpopulated. If galaxies only merge twice, then the faint-end slope is too steep. If galaxies merge four times, then the faint end turns over a little bit too rapidly but the bright end is somewhat above the observations yet does not extend to the brightest magnitudes seen in EDisCS.

These remaining challenges may imply that our model is too simplistic in its treatment of the mass ratios of mergers. For example, in a perfect world the mass ratios should be drawn from the LFs of infalling galaxies and not from the general field population. Also, De Lucia et al. (2012) find that major mergers of massive galaxies in clusters may be preferred based on their results using *N*-body simulations with a semianalytic galaxy formation model. An additional potentially important unmodeled ingredient could the inclusion of the rapid buildup of stellar mass in massive cluster galaxies that are undergoing significant star formation but which must cease their star formation soon after we observe them (Tran et al. 2010). Since the number of dusty star-forming galaxies increases rapidly toward higher redshift, both in the field (e.g., Le Floc'h et al. 2005) and in clusters (Saintonge et al. 2008; Finn et al. 2010), their rapid quenching may be a plausible mechanism to build up the bright end of the red-sequence LF.

It is worth noting that the exact number of mergers needed to match the LF is affected greatly by the slope of the faint end of the blue field LF. If we assume $\alpha = -1.0$ instead of $-1.39$ as in Salimbeni et al. (2008), then the required number of mergers goes down to one to two. The results of this model are also dependent on the faint limit from which we draw field galaxies. We use a faint limit of $-14$ but note that going to $-16$ would require two mergers to sufficiently deplete the faint end of the LF. The results are less dependent on the SFH parameters $t_{\rm cut}$, $t_{\rm delay}$, and $A_i$. For example, $t_{\rm cut} < 2$ Gyr and $A_i < 0.5$ both tend to favor four mergers, with three being ruled out.[13]

The importance of merging in growing the red sequence is consistent with Papovich et al. (2012) and Lotz et al. (2011) who study this cluster with Wide Field Camera 3 (WFC3) imaging from the CANDELS program. Lotz et al. (2011) found that XMM-LSS J02182-05102 has a $\sim$10 times higher merger rate than analogously selected galaxies in the coeval field, and that the close pairs are dominated by galaxies with a high-mass ratio, i.e., minor mergers. The merger rate cited by Lotz et al. (2011) is 2 Gyr$^{-1}$, which is consistent with our estimate of 1 Gyr$^{-1}$ given the considerable uncertainties in both estimates, e.g., in the dependence of our derived merger rate on the field LF. In addition, Papovich et al. (2012) found using the same CANDELS data that the massive red-sequence galaxies in XMM-LSS J02182-05102 require extensive dissipationless, and perhaps minor, mergers in order to simultaneously match the stellar mass, size, ellipticity, and color of cluster red-sequence galaxies at $z < 1$.

There is some direct evidence for merging of red-sequence galaxies in a merging cluster system at $z = 0.8$ (van Dokkum et al. 1999; Tran et al. 2005). Likewise, White et al. (2007) found that to evolve the Halo Occupation Distribution for red luminous satellite galaxies (i.e., cluster red-sequence galaxies) from $z = 0.9$ to 0.5 requires that 1/3 of these galaxies must merge or undergo disruption in massive halos. This is again broadly consistent with the scenario that we propose here as the White et al. (2007) study includes redshifts where the growth in the red sequence has become more gradual. While merging is unlikely in a relaxed massive cluster due to the high velocities, XMM-LSS J02182-05102 will be rapidly growing with time, accreting other clusters and groups along the way. It is not relaxed, which implies that the galaxy–galaxy velocities may be lower than expected given the cluster mass. The relative velocities in the infalling groups will also be lower than in the final cluster and at group scales the merging cross-section may be quite high. Indeed Tran et al. (2008) find that the massive red galaxies in a set of merging groups at $z \sim 0.37$ are themselves experiencing dissipationless mergers that will significantly grow their mass. By $z = 0.8$ the most massive clusters in EDisCS have high-velocity dispersions (Milvang-Jensen et al. 2008), detected intracluster light (Guennou et al. 2012), and strong gravitational lensing (White et al. 2005), implying that the cross-section for merging may be much lower.

### 6.2. Additional Caveats

Our main uncertainty results from this study being based on one high-redshift cluster. As pointed out in Section 5.2, there are differences in the LF of massive clusters at $0.8 < z < 1.1$ and we can expect that these differences might be more extreme in the less-developed cluster population at $z > 1.5$. Obviously, having larger samples of high-redshift clusters with deep NIR data will be crucial if we wish to obtain a representative picture of galaxy evolution in clusters at these epochs.

An additional uncertainty in our result regards the identification of red-sequence galaxies with passively evolving ones. At $z = 0.8$, this is true at the $\sim$85% level (G. H. Rudnick et al. 2012, in preparation). At $z = 1.62$, Tran et al. (2010) found that some of the red-sequence galaxies were 24 $\mu$m emitters, indicating that a small number of red galaxies could be dusty star formers. Papovich et al. (2012) and Quadri et al. (2012) used combinations of rest-frame optical/NIR colors to separate red galaxies that are quiescent from those that are obscured star formers (see also Williams et al. 2009) and found that the contamination on the red sequence from dust-obscured objects is $\sim$20% for bright red galaxies. Given the similar fractions of obscured red galaxies at both redshifts, we conclude that this will not cause a significant error in our conclusions.

The mass estimate for our cluster is also uncertain, with a range between measurements of $M \sim 7.7 \times 10^{13}$ and $1 \times 10^{14} \mathcal{M}_{\odot}$. We adopted the lower of these two—from the X-ray detection—for the analysis in this paper. If we instead chose the mean of these two masses, then the projected mass growth tracks (yellow band in Figure 3) would shift upward but remain roughly parallel to the original. The likely descendant clusters at $z \sim 0.6$ would then be the most massive clusters at every epoch with $M > 10^{15} M_{\odot}$ although in reality such extreme descendants are unlikely due to the steepness of the cluster mass function. The EDisCS LF shape is not dependent on cluster mass (Rudnick et al. 2009), and so the observed lack of evolution in the shape should remain unchanged regardless of the expected descendants. If we adopt the mean mass, then the expected luminosity evolution in Section 5.3 and Figure 5 would be a factor six increase to $z \sim 0.6$ and almost no luminosity evolution

[13] $A_i = 0.7$ corresponds to the typical opacity of galactic disks.

to $z = 0$. As this is very extreme, we are further confident that the lower mass estimate is more appropriate.

A final caveat is our reliance on statistical background subtraction to determine membership. These should have equal or greater reliability when compared to photometric redshifts (Section 5.1), but spectroscopic redshifts are indeed sparse and will help to improve the constraints on the LF, especially at the bright end where continuum redshifts are feasible. Ample spectroscopy will also allow us to better measure the velocity dispersion and dynamical state of the cluster. Likewise, deep medium-band NIR imaging with 6 or 8 m telescopes can provide very precise photometric redshifts that would improve our analysis (Whitaker et al. 2011).

## 7. SUMMARY AND CONCLUSION

We have presented the rest-frame *i*-band LF of red-sequence galaxies of XMM-LSS J02182-05102, a cluster at $z = 1.62$, as measured using deep HAWK-I observations from the VLT and a $K_s$-selected catalog. At this redshift $Y-J$ straddles the Balmer/4000 Å break and $K_s$ is near in wavelength to rest-frame *i*. Our conclusions are as follows.

1. XMM-LSS J02182-05102 has a strong red sequence at bright magnitudes. Starting well brighter than our 90% completeness limit, we find a lack of faint red galaxies. This conclusion is not dependent on our membership identification scheme as these galaxies simply do not exist in this area of the sky. The cluster red sequence hosts the objects with the reddest observed colors in this field and there are very few at faint magnitudes.
2. We derive an LF for the red-sequence cluster members and compare it to analogously constructed LFs for clusters at $z = 0$ from SDSS and $0.4 < z < 0.8$ from EDisCS. When corrected for passive evolution in the luminosities, we find that the shape of the XMM-LSS J02182-05102 LF is indistinguishable from the cluster red-sequence LF at $z = 0.7$ and exhibits the same turnover to faint magnitudes that has been noted by other authors in $z < 1$ clusters. At $z < 0.7$, the faint end of the LF starts to rise and has a near flat slope at $z = 0$. We also find that XMM-LSS J02182-05102 has a lack of luminous red galaxies when compared to clusters from EDisCS.
3. The integral of the measured red-sequence LF shows that $L_{\rm tot,RS}$ for XMM-LSS J02182-05102 is as high as the most luminous EDisCS cluster at $0.4 < z < 0.8$ and the most luminous clusters in SDSS. However, when the expected evolution in the stellar mass-to-light ratio is accounted for, XMM-LSS J02182-05102 has at least three times less stellar mass on the red sequence compared with its likely descendant clusters in SDSS and a factor of two less stellar mass than its likely descendants in EDisCS.
4. We attempt to explain the large growth in the total luminosity between $z = 1.62$ and $z = 0.6$ while simultaneously preventing the buildup of faint red galaxies and also growing massive red ones. We test a simple model in which the cluster accretes galaxies from the blue field population that are quenched and then merge on the red sequence. If every cluster red-sequence galaxy merges ~3–4 times with another red-sequence galaxy, we can satisfy all of the above constraints. This corresponds to a merger rate of $\sim 1\ {\rm Gyr}^{-1}$ integrated over all mass ratios. This also agrees with independent merger rates from this cluster.

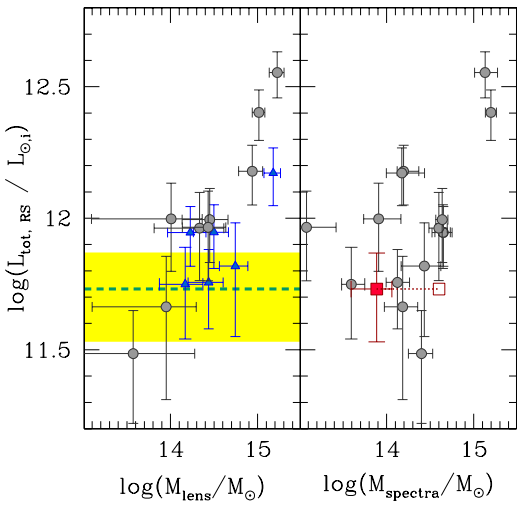


**Figure 7.** Comparison of the dynamical and weak-lensing mass with the integral of the red-sequence luminosity $L_{\rm tot,RS}$. The circle and triangle points are values for the EDisCS clusters $0.4 < z < 0.8$. Left panel: the EDisCS masses are derived from weak-lensing estimates (Clowe et al. 2006), where the blue points are those where substructures may contaminate the lensing signal. The horizontal dashed line and yellow band (left panel) and red point (right panel) give $L_{\rm tot,RS}$ and its uncertainty for XMM-LSS J02182-05102, where the luminosities have been passively faded to $z = 0.6$. Right panel: the EDisCS masses in this panel have been derived from the velocity dispersion using 30–50 members per system from Milvang-Jensen et al. (2008). The red solid square represents the X-ray-derived mass for XMM-LSS J02182-05102 (Pierre et al. 2012). The open square connected to the solid by a dotted line indicates the dynamical mass estimate from Papovich et al. (2010). The disagreement between the two likely reflects the unrelaxed dynamical state of the system. All luminosities are computed in a circular aperture with a radius of 0.75 physical Mpc. The EDisCS luminosities have all had a small passive evolution correction to $z = 0.6$. The correlation of $L_{\rm tot,RS}$ and cluster mass is significant for lensing mass, but less so for mass from the velocity dispersions.

There are some limitations to our analysis. First, our membership information is limited due to the difficulty in obtaining spectroscopic membership information. NIR spectrographs on 6 and 8 m telescopes will be crucial here. We also only have one cluster with an LF of moderate S/N. Obviously, increasing the sample of clusters will allow for a more precise determination of the mean cluster LF at these redshifts and will let us determine whether XMM-LSS J02182-05102 is typical of the high-redshift cluster population.

G.H.R. thanks Hans-Walter Rix and the Max-Planck-Institute for Astronomy in Heidelberg for their warm hospitality during work on parts of this paper. This material is based upon work supported by the National Science Foundation under Award No. EPS-0903806 and matching support from the State of Kansas through Kansas Technology Enterprise Corporation. The authors thank Chris Lidman for useful discussions regarding the processing of HAWK-I data.

## APPENDIX

## THE USE OF THE INTEGRATED RED-SEQUENCE LIGHT AS AN ESTIMATOR OF THE DYNAMICAL MASS

Since the dynamical state of our cluster is likely not relaxed, we seek to estimate the mass using a different method. In Figure 7, we show the correlation of $L_{\rm tot,RS}$ in an $r = 0.75$ Mpc aperture versus weak-lensing mass (Clowe et al. 2006) and mass derived from the velocity dispersion (Milvang-Jensen et al. 2008) for the EDisCS clusters at $0.4 < z < 0.8$. There is a clear

correlation between lensing mass and $L_{\rm tot,RS}$ but a significantly poorer relation with mass derived from the velocity dispersion, even though this dispersion is measured from 30 to 50 members. The horizontal line shows the value for XMM-LSS J02182-05102, where we have corrected the luminosities for passive evolution to $z = 0.6$. If we assume the same ratio of dark matter mass to stellar mass on the red sequence at $z = 0.6$ and $z = 1.62$, then it would appear that XMM-LSS J02182-05102 has $M \sim 2.5 \times 10^{14}\ M_{\odot}$, which is in excellent agreement with the value of $M \sim (1\text{–}4) \times 10^{14}\ M_{\odot}$ from Papovich et al. (2010) and Pierre et al. (2012) as determined from the X-ray luminosity on the low side and the very uncertain velocity dispersion ($\sigma = 860 \pm 490\ \mathrm{km\ s^{-1}}$) on this high side. This opens the possibility of using $L_{\rm tot,RS}$ as a proxy for mass in clusters that we are now selecting with this method, but which do not have spectroscopy sufficient to determine a velocity dispersion.

## REFERENCES


Balogh, M. L., Navarro, J. F., & Morris, S. L. 2000, ApJ, 540, 113
Bell, E. F., Wolf, C., Meisenheimer, K., et al. 2004, ApJ, 608, 752
Blanton, M. R. 2006, ApJ, 648, 268
Bower, R. G., Kodama, T., & Terlevich, A. 1998, MNRAS, 299, 1193
Bower, R. G., Lucey, J. R., & Ellis, R. S. 1992, MNRAS, 254, 601
Brammer, G. B., Whitaker, K. E., van Dokkum, P. G., et al. 2009, ApJ, 706, L173
Brammer, G. B., Whitaker, K. E., van Dokkum, P. G., et al. 2011, ApJ, 739, 24
Brown, M. J. I., Dey, A., Jannuzi, B. T., et al. 2007, ApJ, 654, 858
Brunner, R. J., & Lubin, L. M. 2000, AJ, 120, 2851
Bullock, J. S., Kolatt, T. S., Sigad, Y., et al. 2001, MNRAS, 321, 559
Bundy, K., Ellis, R. S., Conselice, C. J., et al. 2006, ApJ, 651, 120
Calzetti, D., Armus, L., Bohlin, R. C., et al. 2000, ApJ, 533, 682
Casali, M., Pirard, J.-F., Kissler-Patig, M., et al. 2006, Proc. SPIE, 6269, 62690W
Cassata, P., Cimatti, A., Kurk, J., et al. 2008, A&A, 483, L39
Cimatti, A., Daddi, E., & Renzini, A. 2006, A&A, 453, L29
Clowe, D., Schneider, P., Aragón-Salamanca, A., et al. 2006, A&A, 451, 395
Coil, A. L., Newman, J. A., Croton, D., et al. 2008, ApJ, 672, 153
Collins, C. A., Stott, J. P., Hilton, M., et al. 2009, Nature, 458, 603
Cox, T. J., Primack, J., Jonsson, P., & Somerville, R. S. 2004, ApJ, 607, L87
Croton, D. J., Springel, V., White, S. D. M., et al. 2006, MNRAS, 365, 11
Daddi, E., Dickinson, M., Chary, R., et al. 2005a, ApJ, 631, L13
Daddi, E., Renzini, A., Pirzkal, N., et al. 2005b, ApJ, 626, 680
De Lucia, G., & Blaizot, J. 2007, MNRAS, 375, 2
De Lucia, G., Poggianti, B. M., Aragón-Salamanca, A., et al. 2004, ApJ, 610, L77
De Lucia, G., Poggianti, B. M., Aragón-Salamanca, A., et al. 2007, MNRAS, 374, 809
De Lucia, G., Weinmann, S., Poggianti, B. M., Aragón-Salamanca, A., & Zaritsky, D. 2012, MNRAS, 423, 1277
Faber, S. M., Willmer, C. N. A., Wolf, C., et al. 2007, ApJ, 665, 265
Finn, R. A., Desai, V., Rudnick, G., et al. 2010, ApJ, 720, 87
Gabor, J. M., & Davé, R. 2012, MNRAS, submitted (arXiv:1202.5315)
Gallazzi, A., Charlot, S., Brinchmann, J., & White, S. D. M. 2006, MNRAS, 370, 1106
Gilbank, D. G., Yee, H. K. C., Ellingson, E., et al. 2008, ApJ, 673, 742
Guennou, L., Adami, C., Da Rocha, C., et al. 2012, A&A, 537, A64
Gunn, J. E., & Gott, J. R. I. 1972, ApJ, 176, 1
Hilton, M., Stanford, S. A., Stott, J. P., et al. 2009, ApJ, 697, 436
Kauffmann, G., Heckman, T. M., White, S. D. M., et al. 2003, MNRAS, 341, 33
Kriek, M., van der Wel, A., van Dokkum, P. G., Franx, M., & Illingworth, G. D. 2008, ApJ, 682, 896
Labbé, I., Franx, M., Rudnick, G., et al. 2003, AJ, 125, 1107
Labbé, I., Huang, J., Franx, M., et al. 2005, ApJ, 624, L81
Larson, R. B., Tinsley, B. M., & Caldwell, C. N. 1980, ApJ, 237, 692
Lauer, T. R. 1988, ApJ, 325, 49
Le Floc'h, E., Papovich, C., Dole, H., et al. 2005, ApJ, 632, 169
Lidman, C., Rosati, P., Tanaka, M., et al. 2008, A&A, 489, 981
Lotz, J. M., Papovich, C., Faber, S. M., et al. 2011, ApJ, submitted
McGee, S. L., Balogh, M. L., Wilman, D. J., et al. 2011, MNRAS, 413, 996
McIntosh, D. H., Bell, E. F., Rix, H.-W., et al. 2005, ApJ, 632, 191
McNamara, B. R., & Nulsen, P. E. J. 2007, ARA&A, 45, 117
Milvang-Jensen, B., Noll, S., Halliday, C., et al. 2008, A&A, 482, 419
Papovich, C. 2008, ApJ, 676, 206
Papovich, C., Basset, R., Lotz, J. M., et al. 2012, ApJ, 750, 93
Papovich, C., Momcheva, I., Willmer, C. N. A., et al. 2010, ApJ, 716, 1503
Pierre, M., Clerc, N., Maughan, B., et al. 2012, A&A, 540, A4
Pirard, J.-F., Kissler-Patig, M., Moorwood, A., et al. 2004, Proc. SPIE, 5492, 1763
Poggianti, B. M., von der Linden, A., De Lucia, G., et al. 2006, ApJ, 642, 188
Quadri, R., Williams, R., Franx, M., & Hildebrandt, H. 2012, ApJ, 744, 88
Rines, K., Finn, R., & Vikhlinin, A. 2007, ApJ, 665, L9
Rudnick, G., Rix, H.-W., Franx, M., et al. 2003, ApJ, 599, 847
Rudnick, G., von der Linden, A., Pelló, R., et al. 2009, ApJ, 700, 1559
Saintonge, A., Tran, K.-V. H., & Holden, B. P. 2008, ApJ, 685, L113
Salimbeni, S., Giallongo, E., Menci, N., et al. 2008, A&A, 477, 763
Schechter, P. 1976, ApJ, 203, 297
Skelton, R. E., Bell, E. F., & Somerville, R. S. 2012, ApJ, 753, 44
Springel, V., Di Matteo, T., & Hernquist, L. 2005a, ApJ, 620, L79
Springel, V., White, S. D. M., Jenkins, A., et al. 2005b, Nature, 435, 629
Stott, J. P., Collins, C. A., Burke, C., Hamilton-Morris, V., & Smith, G. P. 2011, MNRAS, 414, 445
Stott, J. P., Collins, C. A., Sahlén, M., et al. 2010, ApJ, 718, 23
Stott, J. P., Smail, I., Edge, A. C., et al. 2007, ApJ, 661, 95
Tanaka, M., Finoguenov, A., Kodama, T., et al. 2008, A&A, 489, 571
Tanaka, M., Finoguenov, A., & Ueda, Y. 2010, ApJ, 716, L152
Tanaka, M., Kodama, T., Arimoto, N., et al. 2005, MNRAS, 362, 268
Taylor, E. N., Franx, M., van Dokkum, P. G., et al. 2009, ApJ, 694, 1171
Thomas, D., Maraston, C., Bender, R., & Mendes de Oliveira, C. 2005, ApJ, 621, 673
Thomas, D., Maraston, C., Schawinski, K., Sarzi, M., & Silk, J. 2010, MNRAS, 404, 1775
Toft, S., van Dokkum, P., Franx, M., et al. 2007, ApJ, 671, 285
Trager, S. C., Faber, S. M., & Dressler, A. 2008, MNRAS, 386, 715
Tran, K.-V. H., Moustakas, J., Gonzalez, A. H., et al. 2008, ApJ, 683, L17
Tran, K.-V. H., Papovich, C., Saintonge, A., et al. 2010, ApJ, 719, L126
Tran, K.-V. H., van Dokkum, P., Franx, M., et al. 2005, ApJ, 627, L25
Trujillo, I., Förster Schreiber, N. M., Rudnick, G., et al. 2006, ApJ, 650, 18
van der Wel, A., Franx, M., van Dokkum, P. G., et al. 2005, ApJ, 631, 145
van der Wel, A., Holden, B. P., Zirm, A. W., et al. 2008, ApJ, 688, 48
van Dokkum, P. G., Franx, M., Fabricant, D., Kelson, D. D., & Illingworth, G. D. 1999, ApJ, 520, L95
van Dokkum, P. G., Franx, M., Kriek, M., et al. 2008, ApJ, 677, L5
Wechsler, R. H., Bullock, J. S., Primack, J. R., Kravtsov, A. V., & Dekel, A. 2002, ApJ, 568, 52
Whiley, I. M., Aragón-Salamanca, A., De Lucia, G., et al. 2008, MNRAS, 387, 1253
Whitaker, K. E., Labbé, I., van Dokkum, P. G., et al. 2011, ApJ, 735, 86
Whitaker, K. E., van Dokkum, P. G., Brammer, G., et al. 2010, ApJ, 719, 1715
White, M., Zheng, Z., Brown, M. J. I., Dey, A., & Jannuzi, B. T. 2007, ApJ, 655, L69
White, S. D. M., Clowe, D. I., Simard, L., et al. 2005, A&A, 444, 365
Williams, R. J., Quadri, R. F., Franx, M., van Dokkum, P., & Labbé, I. 2009, ApJ, 691, 1879
Zirm, A. W., van der Wel, A., Franx, M., et al. 2007, ApJ, 656, 66